Research Article

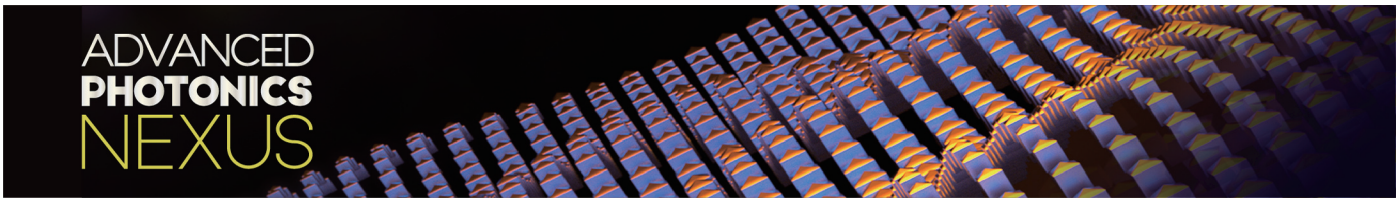

Orbital angular momentum comb generation from azimuthal binary phases

Shiyao Fu,[a,b,c,*] Zijun Shang,[a,b,c] Lan Hai,[a,b,c] Lei Huang,[a,b,c] Yanlai Lv,[a,b,c] and Chunqing Gao[a,b,c,*]
[a]Beijing Institute of Technology, School of Optics and Photonics, Beijing, China
[b]Ministry of Industry and Information Technology of the People's Republic of China, Key Laboratory of Information Photonics Technology, Beijing, China
[c]Ministry of Education of the People's Republic of China, Key Laboratory of Photoelectronic Imaging Technology and System, Beijing, China

Abstract. Since Allen et al. demonstrated 30 years ago that beams with helical wavefronts carry orbital angular momentum (OAM), the OAM of beams has attracted extensive attention and stimulated lots of applications in both classical and quantum physics. Akin to an optical frequency comb, a beam can carry multiple various OAM components simultaneously. A series of discrete, equally spaced, and equally weighted OAM modes comprise an OAM comb. Inspired by the spatially extended laser lattice, we demonstrate both theoretically and experimentally an approach to producing OAM combs through azimuthal binary phases. Our study shows that transition points in the azimuth determine the OAM distributions of diffracted beams. Multiple azimuthal transition points lead to a wide OAM spectrum. Moreover, an OAM comb with any mode spacing is achievable through reasonably setting the position and number of azimuthal transition points. The experimental results fit well with theory. This work presents a simple approach that opens new prospects for OAM spectrum manipulation and paves the way for many applications including OAM-based high-security encryption and optical data transmission, and other advanced applications.

Keywords: orbital angular momentum; orbital angular momentum comb; azimuthal binary phase.

Received Apr. 9, 2022; revised manuscript received May 7, 2022; accepted for publication May 27, 2022; published online Jun. 29, 2022.

[DOI: 10.1117/1.APN.1.1.016003]

1 Introduction

Similar to macroscopic objects, particles such as photons,[1] electrons,[2] and neutrons[3] can also carry angular momentum. The angular momentum of a photon is of two types, with the spin angular momentum (SAM) corresponding to circular polarization[4] and the orbital angular momentum (OAM) determining the helical wavefronts of a beam.[5] Actually, OAM is an inherent feature of a beam whose complex amplitude comprises a helical term $\exp(il\varphi)$, where l is the OAM eigenvalue and known as the topological charge associated with an OAM value $l\hbar$ ($\hbar$ is the reduced Planck's constant) per photon, and φ denotes the azimuthal angle.[6,7] One or more phase singularities determined by multiple OAM components are present for an OAM beam, thus leading to a doughnut-shaped transverse intensity.[8] OAM offers an additional degree of freedom and leads to new possibilities for photonics research. Over the past 30 years, beams carrying OAM have found a wide variety of applications, including large-capacity communications,[9–13] rotation detection,[14–16] optical tweezers and manipulation,[17,18] imaging,[19] gravitational wave detection,[20,21] and quantum information processing.[22,23]

Previous research has provided a variety of schemes to generate OAM beams, such as direct output from a laser[24–28] or endowing a Gaussian beam with spiral phases outside the laser resonator.[29–34] Nevertheless, most of the aforementioned methods concentrate only on the generation of single or simple multiplexed OAM modes. Beams carrying a wide series of discrete, equally spaced, and manipulated OAM components with identical intensities, namely the OAM comb, are conducive to current OAM-based scenarios. For instance, multiplexed OAM multicasting enables one-to-multichannel data transmission, further enlarging the dimensions of OAM-based optical communications.[35] The OAM comb can also act as a flexible key for holographic encryption and decryption.[36,37] Currently,

*Address all correspondence to Shiyao Fu, fushiyao@bit.edu.cn; Chunqing Gao, gao@bit.edu.cn

schemes such as mode iteration,[38] pattern-search algorithm,[39] adaptive modification,[40] and pinhole plates[41] have been reported to tailor the OAM spectrum or produce an OAM comb. However, these schemes may face problems such as long response or calculation time, complex systems, and lower diffraction efficiency, which motivated us to develop a simple, flexible, and functional approach to selectively manipulate OAM combs.

In this study, we overcome the aforementioned limitations by demonstrating a specially designed azimuthal 0-π binary phase-only grating for the selective manipulation of OAM combs. Several transition points were embedded in a spiral phase along the azimuth to tailor the OAM spectrum of the diffractive beams. The number and position of the azimuthal transition points were optimized to produce arbitrary OAM combs, where the optimized results were fixed and could be employed for various scenarios at any time. A proof-of-principle experiment was performed to demonstrate the performance of the proposed azimuthal binary-phase gratings. These favorable results were in good agreement with our simulations. This study offers a real-time, flexible, simple, and accurate method for generating beams with complicated OAM spectra, which paves the way for classical/quantum optical communications, holographic encryption and decryption, and other advanced applications in the future.

2 Results and Discussion

2.1 Azimuthal Phase Modulation: From Continuation to Binarization

Previous studies have illustrated that a continuous azimuthal phase, namely a spiral phase plate (SPP), can bring a pure single OAM mode for the incident beams.[29] In other words, such spiral phase $P_{\text{spp}} = l\varphi \bmod 2\pi$ with $|l|$ nodal lines can transform a Gaussian beam into an OAM beam with topological charge l. As displayed in Fig. 1(a), if we binarize the continuous azimuthal phase as 0 and π with the binarization threshold $P_{\text{th}} = \pi$:

$$P_B = \begin{cases} 0, & \text{if } P_{\text{spp}} < P_{\text{th}} \\ \pi, & \text{if } P_{\text{spp}} \geq P_{\text{th}} \end{cases}, \tag{1}$$

where P_B denotes the phase distribution of the azimuthal binary phase, one can obtain a petal-like pattern with $|2l|$ petals. The OAM spectrum of such beam can be diagnosed through helical harmonic decomposition,[42] where two main OAM components with a topological charge $\pm l$ are present. Some high-order helical harmonic terms $\pm Nl$ (N is an integer) also emerged. Such phenomena imply that the binarized azimuthal phase can produce multiple symmetric OAM components with respect to the fundamental mode $l = 0$. If the binarization threshold replaced by other values belongs to section $[0,2\pi)$, the OAM spectra of diffractive beams turn out to be diversified. As displayed in Fig. 1(b), we choose seven various binarization thresholds P_{th} as $\pi/4$, $\pi/2$, $3\pi/4$, π, $5\pi/4$, $3\pi/2$, and $7\pi/4$ to binarize the continuous azimuthal phase with one nodal line ($l = 1$), and analyze the OAM spectra of the diffraction beams. Obviously, the OAM spectra can be tuned under various binarization thresholds P_{th}. In addition, there is an azimuthal transition point φ_κ in each binary phase, the position of which is surely determined by P_{th}, as shown in the second line of Fig. 1(b). That is, one can understand that the positions of azimuthal transition points induce redistributions of the azimuthal phase, giving rise to various OAM spectra. Meanwhile, the complementary two binary phase distributions ($P_{B1} + P_{B2} = 2\pi$) lead to the same OAM spectra, resulting from the relative phase difference of 0-π binarized phase modulation.

2.2 Azimuthal Binary Phase with Multiple Transition Points

Next, we discuss what happens if multiple azimuthal transition points are brought in. The phase distribution of a 0-π binary phase-only grating with $(K + 1)$ various azimuthal transition points within one grating period reads

$$P_B(\varphi) = \pi \sum_{\kappa=0}^{K} (-1)^{\kappa+1} \text{rect}\left(\frac{\varphi}{\varphi_\kappa} - 0.5\right), \varphi \in [0,2\pi), \tag{2}$$

with φ_κ as the κ'th transition point and $\kappa = 0,1,2,\ldots,K$. The diffraction field of such a grating for an incident Gaussian beam can be calculated approximatively through Fourier transformation (Supplementary Note 1), which contains multiple diverse OAM components. As an example, Fig. 2 displays the evolution of the obtained OAM spectra with respect to azimuthal transition points. The first, second, third, and fourth lines show the transition points, the corresponding azimuthal binary phase distributions, far-field diffractions, and OAM spectra, respectively. Four azimuthal transition points are chosen here as $\varphi_0 = 0$, $\varphi_1 = 1.4564$, $\varphi_3 = 2.6703$, and $\varphi_4 = 3.3015$. If there are two transition points only, the phase distribution is simple and the obtained OAM spectrum emerges as a hill-shaped envelope. When all the three transition points are introduced, the binary phase gets a little more complicated but the final OAM spectrum turns out to be structured as seven different OAM components whose topological charges range from -3 to $+3$ are present and show nearly equal intensities, i.e., a kind of OAM comb. Such phenomena imply that an azimuthal 0-π binary phase is an effective pathway to tailor OAM combs, providing that the number and value of azimuthal transition points are well selected.

2.3 OAM Comb Manipulation

To produce the desired OAM combs, a feasible way is to find a proper set of transition points. From the scalar diffraction theory, the far-field diffraction E of an incident plane wave can be calculated approximatively by the Fourier transform of the transmittance function of azimuthal binary phases. Thus, E from Eq. (2) reads $E = F[\exp(iP_B)]$, where F denotes Fourier transformation. On the basis of helical harmonic $\exp(il\varphi)$, the diffraction field E can be decomposed into the summation of infinite helical term with various complex weights a_l:[42]

$$E(r,\varphi) = \frac{1}{\sqrt{2\pi}} \sum_{l=-\infty}^{+\infty} a_l \exp(il\varphi). \tag{3}$$

The complex weights in Eq. (3) read

$$a_l = \frac{1}{\sqrt{2\pi}} \int_0^{2\pi} E(r,\varphi) \exp(-il\varphi) \mathrm{d}\varphi. \tag{4}$$

Actually, $|a_l|^2$ corresponds to the intensity of OAM channel l. By now, a mind map of OAM comb manipulation emerges

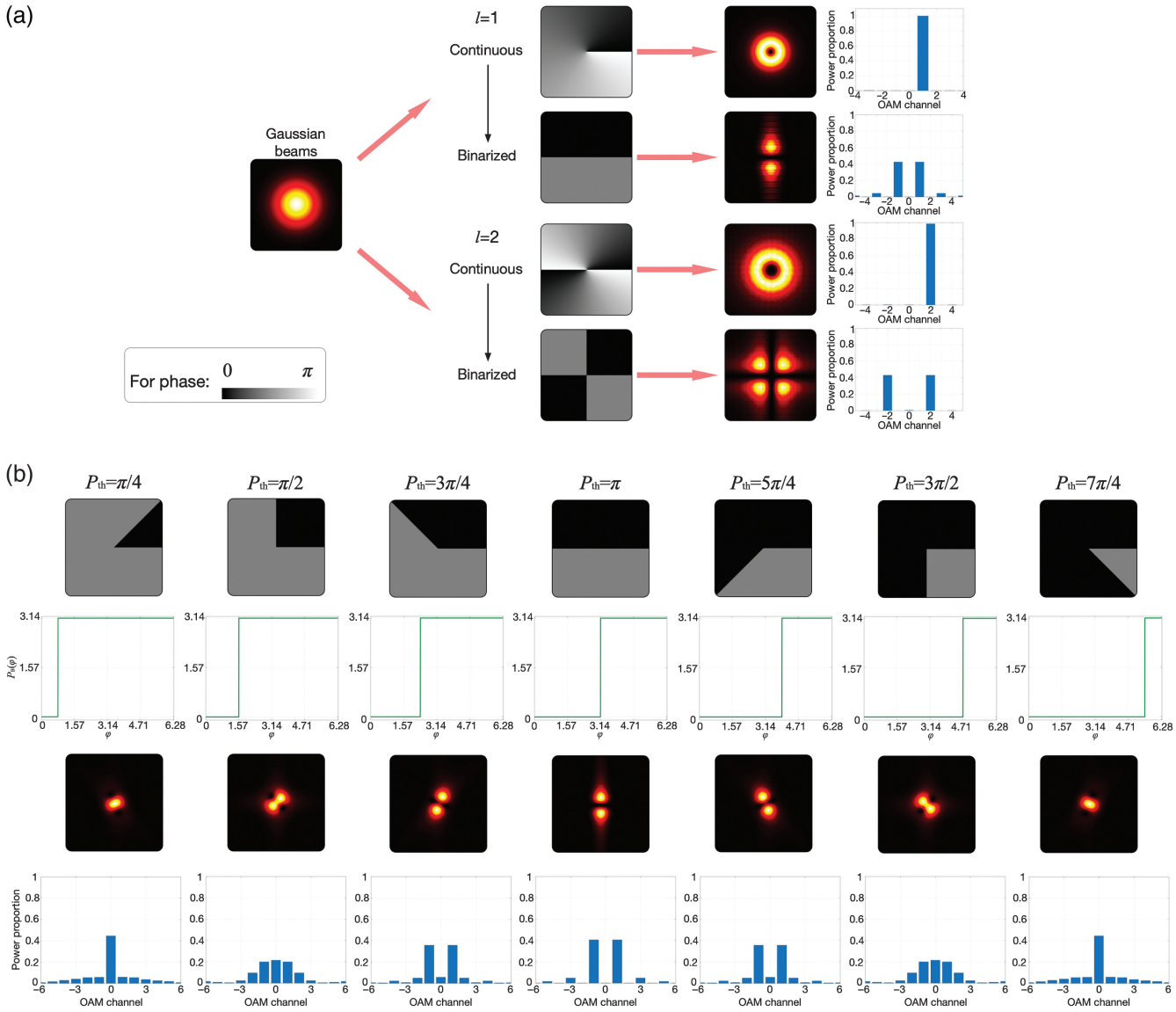

Fig. 1 Binarizing continuous azimuthal phases into 0-π azimuthal binary phases. (a) The binarization of continuous azimuthal phases with one and two nodal lines (the first- and second-order SPPs) under the threshold $P_{\text{th}} = \pi$. The binarized phase can produce symmetric OAM components with respect to $l = 0$ mode, compared with the corresponding continuous azimuthal phases. (b) The 0-π phase binarized under various binarization threshold P_{th} as $\pi/4$, $\pi/2$, $3\pi/4$, π, $5\pi/4$, $3\pi/2$, and $7\pi/4$, respectively. First to fourth lines in panel (b): the phase distribution, the phase versus the azimuthal angle φ, the simulated far-field diffraction pattern, and the corresponding calculated OAM spectrum.

clearly, as the azimuthal transition points lead to azimuthal nodal lines determine the diffraction fields, and such fields further determine the intensity of each OAM channel $|a_l|^2$. In other words, the final OAM spectrum is a function of azimuthal transition points φ_κ as $|a_l|^2 = f(\varphi_\kappa)$ indeed (Supplementary Note 2). To find a proper set $\{\varphi_\kappa\}$ for the desired OAM comb, several evaluation parameters are necessary. Here two parameters are introduced, one of which is the efficiency defined as $\eta = (\Sigma_{l\in\mathbf{L}}|a_l|^2)/\Sigma_{l\in\mathbf{Z}}|a_l|^2$, where $\mathbf{L}$ and $\mathbf{Z}$ denote the set of topological charges of desired OAM comb and the integer set separately. The other is the uniformity as $U = 2\min|a_l|^2/(\max|a_l|^2 + \min|a_l|^2)$, where $l \in \mathbf{L}$, $\min\{\}$ and $\max\{\}$ denote taking the minimum and maximum, respectively. Note that η must be <1 because a single phase-only grating cannot produce coaxial multiplexed OAM modes with desired OAM distributions, and there must be irrelevant and undesired OAM modes.[38] $\{\varphi_\kappa\}$ calculation is available through iteration embedded numerical simulation. In each iteration, one must evaluate the value of η and U to decide how to adjust the transition points set $\{\varphi_\kappa\}$ until an ideal scenario where the finally calculated transition points contribute to highest efficiency η and uniformity U. Usually such process is complex and time-consuming, which incommodes the practical application of OAM comb. Zhou and Liu[43] have already demonstrated numerical

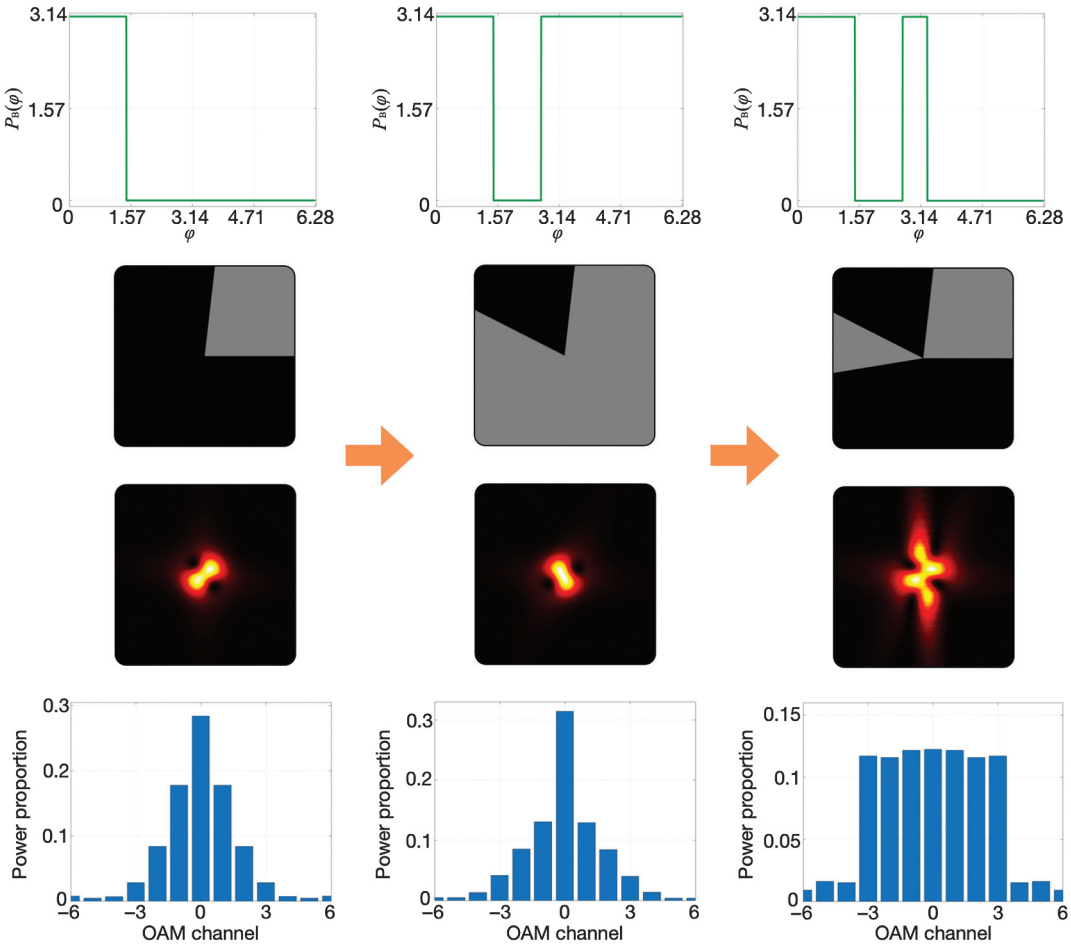

Fig. 2 The evolution of the obtained OAM spectra with respect to azimuthal transition points. Four transition points as $\varphi_0 = 0$, $\varphi_1 = 1.4564$, $\varphi_2 = 2.6703$, and $\varphi_3 = 3.3015$ are introduced orderly in the azimuthal section $[0,2\pi)$ as an example to demonstrate OAM spectrum variation. From top to bottom are the azimuthal transition points, the corresponding azimuthal binary phases, far-field diffraction patterns, and OAM spectra. Obviously, the number and value of transition points determine the final obtained OAM spectra.

solutions for 0-π binary Dammann gratings, which can expand the incident beam along the x direction to achieve a one-dimensional (1D) equal-intensity laser array with both high efficiency and high uniformity. In Ref. 43, multiple lateral (x) transition points are introduced within one grating period T, resulting in multiple presented diffraction orders (x-expanded modes) featured as $\Sigma \exp(i2\pi mx/T)$, where m corresponds to the m'th diffraction order. Here, we move from "x-space" to "φ-space," where the azimuthal (φ) transition points in one azimuthal period ($\Pi = 2\pi$) lead to OAM superposed modes (φ-expanded modes) featured as $\Sigma \exp(il\varphi) = \Sigma \exp(i2\pi l\varphi/\Pi)$. The resulting fields in the above two "spaces" have identical forms. Their only difference is that one expands the incident beam along the x coordinate while the other along the φ coordinate. Such phenomena imply that the numerical solutions given in Ref. 43 are also effective to be employed in the azimuth to produce various OAM superposed modes with equal intensities.

We map the numerical solutions presented in Ref. 43 from "x-space" to "φ-space" (Supplementary Note 3) to generate azimuthal 0-π binary phases, calculate the far-field diffractions through the scalar diffraction theory for incident Gaussian beams, and then analyze the OAM spectra (Supplementary Note 4). As displayed in Fig. 3(a), an azimuthal binary phase can produce nine equal-intensity OAM modes with topological charges ranging from -4 to $+4$. It has six azimuthal transition points as 0, 0.4190, 0.8087, 1.7963, 2.8693, and 3.7127. The efficiency and the uniformity of the obtained OAM comb are calculated as 78.32% and 99.61%, which are high enough for OAM comb manipulation. In addition, we also attempt to generate OAM combs with other OAM mode intervals Δl. Such manipulation is based on the scaling property of the Fourier transform, where if $F\{f(x)\} = F(u)$, then $F\{f(x/a)\} = |a|F(au)$ with a the scale factor. So, here scaling the azimuthal phase φ contributes to $F\{T_B(\varphi/\Delta l)\} \propto \Sigma_l \exp(i\Delta l l\varphi')$, where φ' is the azimuthal angle in the far field. As an example, we scale the azimuthal angle in Fig. 3(a) with scale factors $\Delta l = 2$ and $\Delta l = 3$, and the final obtained OAM combs are given in Figs. 3(b) and 3(c). Note that the OAM comb is present through normalized intensity, where the calculated or experimentally measured intensity of each OAM channel is normalized with respect to the maximum intensity among all the present OAM channels. In both of the two scenarios, there are also nine OAM

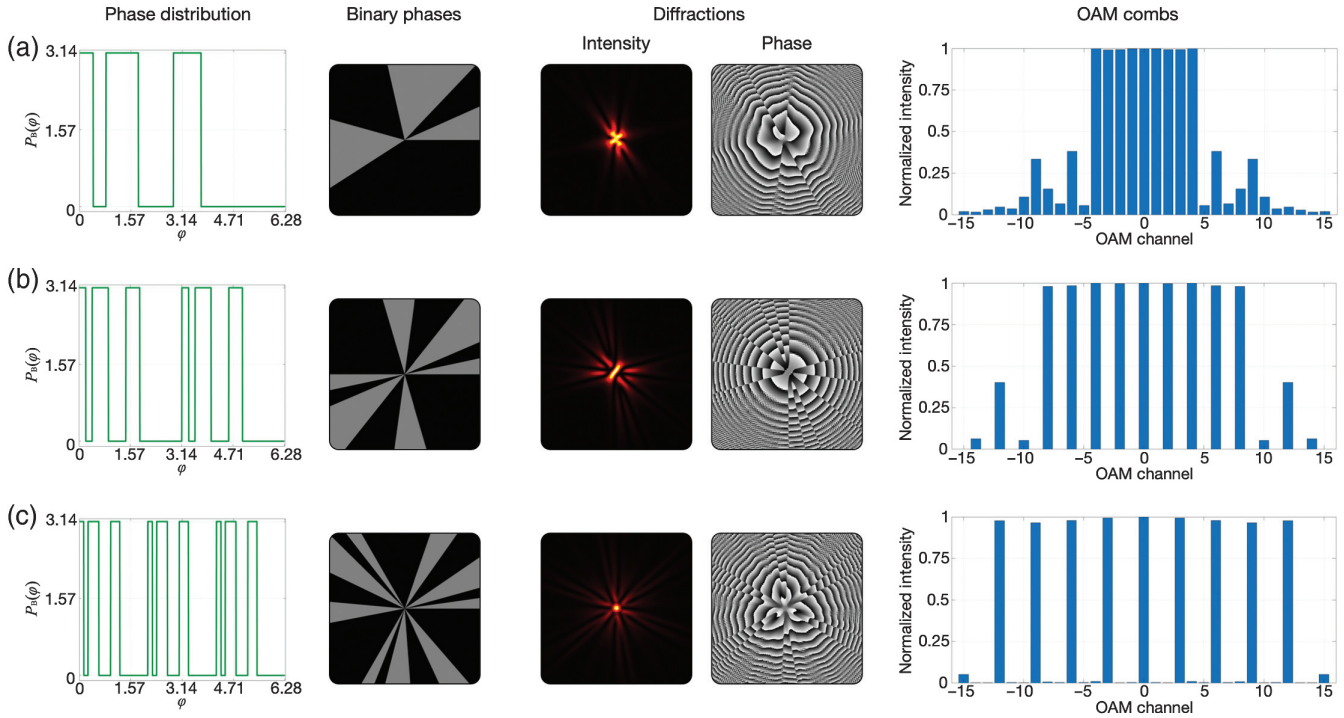

Fig. 3 OAM comb manipulation with various OAM mode intervals. From left to right are azimuthal transition points, the corresponding binary phases, far-field diffractions, and OAM combs, respectively. All the OAM combs in (a), (b), and (c) consist of nine OAM components, but their OAM mode intervals are different as 1, 2, and 3, respectively. The interval difference results by scaling the azimuthal phase φ.

modes with equal intensities. However, their topological charge distributions are totally different; one is -8 to $+8$ with $\Delta l = 2$, the other is -12 to $+12$ with $\Delta l = 3$. Such phenomena illustrate that it is practicable to produce OAM combs with various OAM mode intervals through azimuth scaling and provide a more flexible scheme of OAM comb manipulation. Additionally, OAM range is limited to -15 to $+15$ here. When extending such a present range, in Figs. 3(b) and 3(c) one can see undesired side OAM modes distributions similar to Fig. 3(a), but the only difference is the space between adjacent OAM channels.

Proof-of-principle experiments are also carried out to show the practical operability (Supplementary Notes 5–7). In the experiment, we encode the azimuthal 0-π binary phase onto a liquid-crystal spatial light modulator (SLM) to accomplish the phase-only modulation. The OAM spectra are analyzed with the back-converted method as a series of spiral phases $(l_1, l_2, \ldots, l_N)$, also known as anti-SPPs in some literature, are encoded simultaneously on the SLM and then the intensity of center bright spot is calculated to represent the relative intensity of the OAM channel $-l_1, -l_2, \ldots, -l_N$. We first generate an OAM comb consisting of 64 OAM states ranging from -63 to $+63$ with the OAM mode interval $\Delta l = 2$. The experimentally captured intensity patterns and OAM spectrum and its corresponding simulation results are given in Fig. 4(a). The uniformity of the experimental result is evaluated as 92.04%, which is lower than that of the simulation at 98.16%. In addition, the similarity, which implies the consistency between the experimental and theoretical results suggested by the work[44,45] is evaluated as 96.49%. We also generate an OAM comb consisting of 32 OAM states ranging from -62 to $+62$ with the OAM mode interval $\Delta l = 4$, the results of which are shown in Fig. 4(b). In this case, the uniformities of the experimental and simulated results are 90.95% and 98.86%, respectively, and the similarity is analyzed as 93.36%. The numbers of azimuthal transition points $\{\varphi_\kappa\}$ for the above two cases are 70 and 68 separately (Supplementary Note 6). The measured OAM spectra in the experiment show little difference compared with simulation, where the intensities emerge in some irrelevant OAM channels and some power is likely to leak from desired to undesired OAM components. In fact, such "leakage" is meaningless and makes no physical sense because inevitable interchannel crosstalk is introduced during the data-processing of the back-conversion-based OAM spectrum measurement.

3 Conclusions

We showed that binarizing a spiral phase into 0-π binarization results in multiple OAM components that are symmetric with respect to the fundamental mode ($l = 0$) of equal intensity. In this case, there are two azimuthal transition points constituting the two nodal lines that divide phases 0 and π. When more transition points are introduced, the resulting OAM spectrum becomes more complex. Nevertheless, the OAM distribution can be tailored by adjusting the number and value of azimuthal transition points to accomplish arbitrary OAM comb manipulations. Finding a proper set of azimuthal transition points is crucial for OAM comb manipulation; however, it is complicated because of repetitive iterations. Therefore, based on previous reports on the numerical solutions of lateral transition points to construct a 1D beam lattice that expands the incident beam along the x axis, we build a mapping between the x axis in

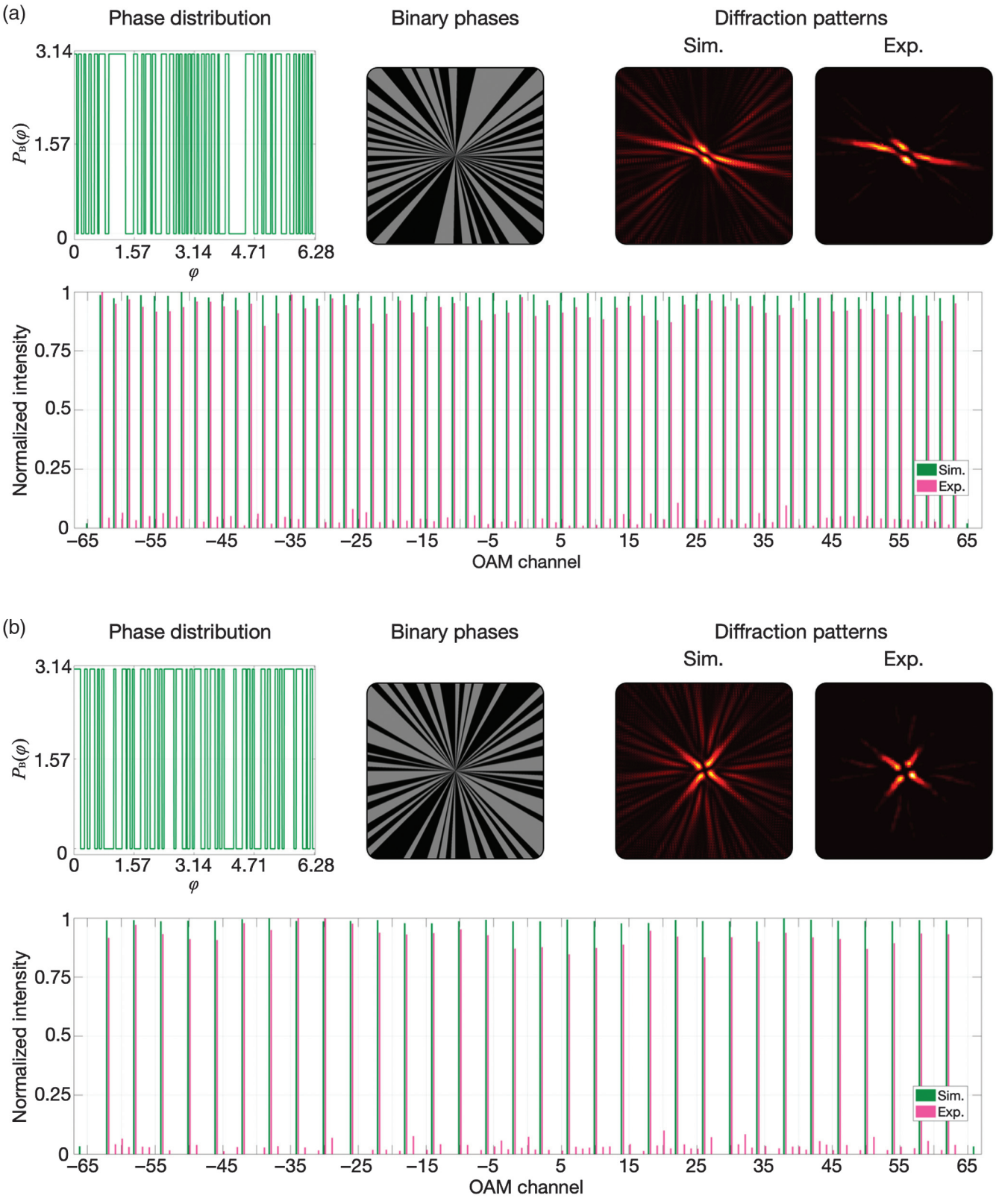

Fig. 4 Experimentally generated OAM combs. (a) Experimental results of an OAM comb consisting of 64 OAM states ranging from −63 to +63 with the OAM mode interval $\Delta l = 2$. (b) Experimental results of an OAM comb consisting of 64 OAM states ranging from −62 to +62 with the OAM mode interval $\Delta l = 4$. In both of the cases the OAM spectra are measured through anti-SPP based OAM back-conversion.

Cartesian coordinates and the φ axis in polar coordinates, thus transforming the optimal solution of transition points along the x axis into that of the azimuth along the φ axis to accomplish a fast binary phase calculation. In the simulation, we successfully produce various OAM combs following the above hypothesis. We also show how to adjust the mode interval between adjacent OAM modes inside the OAM comb by scaling the azimuthal coordinates. In the proof-of-principle experiment, OAM combs consisting of up to 64 OAM components with the largest absolute value of OAM state 63 are generated, whose uniformity reaches 92.04% and fits well with the theory. We also attempt to adjust the OAM mode interval in practice and produce an OAM comb comprising 32 OAM components whose OAM states range from −62 to +62 with a mode interval of 4. The uniformity is evaluated to be 90.95%. The favorable experimental results illustrate that our proposed method exhibits good performance for tailoring OAM combs in practice.

In addition, the OAM states can be shifted by illuminating the 0-π binary phase-only grating with a higher-order optical vortex. Alternatively, this may be done by integrating the l'th order spiral phase with the proposed binary azimuthal phase to shift the OAM components by l, as in Ref. 46. In this manner, OAM combs whose components are asymmetric with respect to the fundamental mode ($l = 0$) can also be achieved.

The ability to generate a beam with a specifically tailored OAM spectrum is crucial for OAM applications; e.g, the unique key of holographic encryption and decryption.[36,37] In addition, the proposed approach provides a convenient method for the practical generation of high-dimensional OAM combs, namely, an available high-dimensional Hilbert space; thus, it can find potential in high-dimensional photon entanglement and will inspire applications in quantum key distribution and quantum teleportation.[47] Iteration methods are typically employed to optimize phase-only gratings to produce a multiplexed OAM beam. However, these complicated processes are time-consuming and may be inconvenient for practical applications. Herein, we demonstrate a simple approach in which azimuthal binary phases are introduced to manipulate arbitrary OAM combs with equal mode intensities. Furthermore, the azimuthal transition points can be easily calculated by mapping the numerical solutions of the binary lateral phases. In summary, our proposal opens new avenues for OAM comb manipulation and lays the foundation for applications in many OAM-based systems.

Acknowledgments

This work is supported by National Natural Science Foundation of China (NSFC) (11834001, 61905012), National Defense Basic Scientific Research Program of China (JCKY2020602C007), and National Postdoctoral Program for Innovative Talents (BX20190036). The authors declare no competing financial interests.

Availability of Data and Materials

The simulated and experimental data that support the works of this study are available from the corresponding authors on reasonable request.

References

1. G. Molina-Terriza, J. P. Torres, and L. Torner, "Twisted photons," *Nat. Phys.* **3**(5), 305–310 (2007).
2. J. Verbeeck, H. Tian, and P. Schattschneider, "Production and application of electron vortex beams," *Nature* **467**(7313), 301–304 (2010).
3. C. W. Clark et al., "Controlling neutron orbital angular momentum," *Nature* **525**(7570), 504–506 (2015).
4. R. A. Beth, "Mechanical detection and measurement of the angular momentum of light," *Phys. Rev.* **50**(2), 115–125 (1936).
5. A. M. Yao and M. J. Padgett, "Orbital angular momentum: origins, behavior and applications," *Adv. Opt. Photonics* **3**(2), 161–204 (2011).
6. L. Allen et al., "Orbital angular-momentum of light and the transformation of Laguerre–Gaussian laser modes," *Phys. Rev. A* **45**(11), 8185–8189 (1992).
7. L. Allen, M. J. Padgett, and M. Babiker, "The orbital angular momentum of light," *Prog. Opt.* **39**, 291–372 (1999).
8. Y. Shen et al., "Optical vortices 30 years on: OAM manipulation from topological charge to multiple singularities," *Light Sci. Appl.* **8**(1), 90 (2019).
9. J. Wang et al., "Terabit free-space data transmission employing orbital angular momentum multiplexing," *Nat. Photonics* **6**(7), 488–496 (2012).
10. N. Bozinovic et al., "Terabit-scale orbital angular momentum mode division multiplexing in fibers," *Science* **340**(6140), 1545–1548 (2013).
11. T. Lei et al., "Massive individual orbital angular momentum channels for multiplexing enabled by Dammann gratings," *Light Sci. Appl.* **4**(3), e257 (2015).
12. M. Krenna et al., "Twisted light transmission over 143 km," *Proc. Natl. Acad. Sci. U. S. A.* **113**(48), 13648–13653 (2016).
13. S. Fu et al., "Demonstration of free-space one-to-many multicasting link from orbital angular momentum encoding," *Opt. Lett.* **44**(19), 4753–4756 (2019).
14. M. P. J. Lavery et al., "Detection of a spinning object using light's orbital angular momentum," *Science* **341**(6145), 537–540 (2013).
15. M. P. J. Lavery et al., "Observation of the rotational Doppler shift of a white-light, orbital- angular-momentum-carrying beam backscattered from a rotating body," *Optica* **1**(1), 1–4 (2014).
16. S. Fu et al., "Non-diffractive Bessel-Gauss beams for the detection of rotating object free of obstructions," *Opt. Express* **25**(17), 20098–20108 (2017).
17. M. Padgett and R. Bowman, "Tweezers with a twist," *Nat. Photonics* **5**(6), 343–348 (2011).
18. Y. Yang et al., "Optical trapping with structured light: a review," *Adv. Photonics* **3**(3), 034001 (2021).
19. X. Qiu et al., "Spiral phase contrast imaging in nonlinear optics: seeing phase objects using invisible illumination," *Optica* **5**(2), 208–212 (2018).
20. M. Granata et al., "Higher-order Laguerre-Gauss mode generation and interferometry for gravitational wave detectors," *Phys. Rev. Lett.* **105**(23), 231102 (2010).
21. N. Andreas, B. Christina, and W. Benno, "Higher-order Laguerre–Gauss modes in (non-) planar four-mirror cavities for future gravitational wave detectors," *Opt. Lett.* **42**(4), 751–754 (2017).
22. J. B. Götte et al., "Light beams with fractional orbital angular momentum and their vortex structure," *Opt. Express* **16**(2), 993–1006 (2008).
23. M. Mafu et al., "Higher-dimensional orbital-angular-momentum-based quantum key distribution with mutually unbiased bases," *Phys. Rev. A.* **88**(3), 032305 (2013).
24. A. Forbes, "Structured light from lasers," *Laser Photonics Rev.* **13**(11), 1900140 (2019).
25. S. Ngcobo et al., "A digital laser for on-demand laser modes," *Nat. Commun.* **4**(1), 2289 (2013).
26. H. Sroor et al., "High-purity orbital angular momentum states from a visible metasurface laser," *Nat. Photonics* **14**, 498–503 (2020).
27. R. Song et al., "Resonantly pumped Er:YAG vector laser with selective polarization states at 1.6 μm," *Opt. Lett.* **45**(16), 4626–4629 (2020).

28. Y. Shen et al., "Structured ray-wave vector vortex beams in multiple degrees of freedom from a laser," *Optica* **7**(7), 820–831 (2020).
29. M. W. Beijersbergen et al., "Helical-wavefront laser beams produced with spiral phase plate," *Opt. Commun.* **112**, 321–327 (1994).
30. A. Forbes, A. Dudley, and M. McLaren, "Creation and detection of optical modes with spatial light modulators," *Adv. Opt. Photonics* **8**(2), 200–227 (2016).
31. L. Marrucci, C. Manzo, and D. Paparo, "Optical spin-to-orbital angular momentum conversion in inhomogeneous anisotropic media," *Phys. Rev. Lett.* **96**(16), 163905 (2006).
32. R. C. Devlin et al., "Arbitrary spin-to-orbital angular momentum conversion of light," *Science* **358**(6365), 896–901 (2017).
33. H. Zhou et al., "High-efficiency, broadband all-dielectric transmission metasurface for optical vortex generation," *Opt. Mater. Express* **9**(6), 2699–2707 (2019).
34. H. Wang, S. Fu, and C. Gao, "Tailoring a complex perfect optical vortex array with multiple selective degrees of freedom," *Opt. Express* **29**(7), 10811–10824 (2021).
35. Y. Zhao et al., "Demonstration of data-carrying orbital angular momentum-based underwater wireless optical multicasting link," *Opt. Express* **25**(23), 28743–28751 (2017).
36. X. Fang, H. Ren, and M. Gu, "Orbital angular momentum holography for high-security encryption," *Nat. Photonics* **14**(2), 102–108 (2020).
37. X. Fang et al., "High-dimensional orbital angular momentum multiplexing nonlinear holography," *Adv. Photonics* **3**(1), 015001 (2021).
38. J. Lin et al., "Collinear superposition of multiple helical beams generated by a single azimuthally modulated phase-only element," *Opt. Lett.* **30**(24), 3266–3268 (2005).
39. L. Zhu and J. Wang, "Simultaneous generation of multiple orbital angular momentum (OAM) modes using a single phase-only element," *Opt. Express* **23**(20), 26221–26233 (2015).
40. S. Li and J. Wang, "Adaptive power-controllable orbital angular momentum (OAM) multicasting," *Sci. Rep.* **5**, 9677 (2015).
41. Y. Yang et al., "Manipulation of orbital-angular-momentum spectrum using pinhole plates," *Phys. Rev. Appl.* **12**(6), 064007 (2019).
42. S. Fu et al., "Universal orbital angular momentum spectrum analyzer for beams," *PhotoniX* **1**(1), 19 (2020).
43. C. Zhou and L. Liu, "Numerical study of Dammann array illuminators," *Appl. Opt.* **34**(26), 5961–5969 (1995).
44. B. Sephton et al., "A versatile quantum walk resonator with bright classical light," *PLoS ONE* **14**(4), e0214891 (2019).
45. G. Ruffato et al., "A compact diffractive sorter for high-resolution demultiplexing of orbital angular momentum beams," *Sci. Rep.* **8**, 10248 (2018).
46. S. Fu et al., "Integrating 5 × 5 Dammann gratings to detect orbital angular momentum states of beams with the range of −24 to +24," *Appl. Opt.* **55**, 1514–1517 (2016).
47. L. Chen, "Quantum discord of thermal two-photon orbital angular momentum state: mimicking teleportation to transmit an image," *Light Sci. Appl.* **10**, 148 (2021).
48. Y. D. Liu et al., "Coherent-mode representation and orbital angular momentum spectrum of partially coherent beam," *Opt. Commun.* **281**, 1968–1975 (2008).
49. C. Schulze et al., "Measurement of the orbital angular momentum density of light by modal decomposition," *New J. Phys.* **15**, 073025 (2013).
50. H. Dammann and E. Klotz, "Coherent optical generation and inspection of two-dimensional periodic structures," *Optica Acta: Int. J. Opt.* **24**(4), 505–515 (1977).
51. J. Jahns et al., "Dammann gratings for laser beam shaping," *Opt. Eng.* **28**(12), 281267 (1989).
52. J. Li, Z. Peng, and Y. Fu, "Diffraction transfer function and its calculation of classic diffraction formula," *Opt. Commun.* **280**, 243–248 (2007).
53. S. Fu et al., "Measurement of orbital angular momentum spectra of multiplexing optical vortices," *Opt. Express* **24**(6), 6240–6248 (2016).
54. M. Mirhosseini et al., "Efficient separation of the orbital angular momentum eigenstates of light," *Nat. Commun.* **4**, 2781 (2013).
55. H. L. Zhou et al., "Orbital angular momentum complex spectrum analyzer for vortex light based on the rotational Doppler effect," *Light Sci. Appl.* **6**, e16251 (2017).

Shiyao Fu is currently an associate professor at Beijing Institute of Technology. He received his PhD in electronic science and technology from Beijing Institute of Technology in 2019. His current research interests cover complex structured fields manipulation, novel solid-state lasers, and their applications in critical engineering. He has published one book and more than 40 peer-reviewed papers. He has 18 authorized patents. He was selected for the national postdoctoral program for Innovative Talents. He won the Wang Da-Heng Optics Prize, and his doctoral dissertation was recognized by the Chinese Institute of Electronics. He is a senior member of the Chinese Optical Society.

Chunqing Gao is a professor in the School of Optics and Photonics, Beijing Institute of Technology, China since 2001. He received his BS degree and MS degree in optics from Beijing Institute of Technology, and received his PhD in physics from Technical University Berlin, Germany. The current research in his group mainly focuses on novel laser systems, laser beam manipulation, and related applications. He has published three books and more than 260 scientific papers in journals and conferences. He has 30 authorized patents in the fields of optics and lasers.

Biographies of the other authors are not available.